



# University of HUDDERSFIELD

## University of Huddersfield Repository

Banitalebi Dehkordi, H., Farzaneh, M., Van Dyke, P. and Kollar, László E.

The effect of droplet size and liquid water content on ice accretion and aerodynamic coefficients of tower legs

### Original Citation

Banitalebi Dehkordi, H., Farzaneh, M., Van Dyke, P. and Kollar, László E. (2013) The effect of droplet size and liquid water content on ice accretion and aerodynamic coefficients of tower legs. *Atmospheric Research*, 132-3. pp. 362-374. ISSN 0169-8095

This version is available at <http://eprints.hud.ac.uk/id/eprint/18938/>

The University Repository is a digital collection of the research output of the University, available on Open Access. Copyright and Moral Rights for the items on this site are retained by the individual author and/or other copyright owners. Users may access full items free of charge; copies of full text items generally can be reproduced, displayed or performed and given to third parties in any format or medium for personal research or study, educational or not-for-profit purposes without prior permission or charge, provided:

- The authors, title and full bibliographic details is credited in any copy;
- A hyperlink and/or URL is included for the original metadata page; and
- The content is not changed in any way.

For more information, including our policy and submission procedure, please contact the Repository Team at: [E.mailbox@hud.ac.uk](mailto:E.mailbox@hud.ac.uk).

<http://eprints.hud.ac.uk/>

# The effect of droplet size and liquid water content on ice accretion and aerodynamic coefficients of tower legs

H. Banitalebi Dehkordi<sup>1</sup>, M. Farzaneh<sup>1</sup>, P. Van Dyke<sup>2</sup> and L. E. Kollar<sup>1</sup>

<sup>1</sup>NSERC/Hydro-Québec/UQAC Industrial Chair on Atmospheric Icing of Power Network Equipment (CIGELE) and Canada Research Chair on Engineering of Power Network Atmospheric Icing (INGIVRE), Université du Québec à Chicoutimi, QC, Canada, ([www.cigele.ca](http://www.cigele.ca))

<sup>2</sup>Hydro-Québec Research Institute (IREQ), Varennes, QC, Canada

## Abstract

An experimental study was conducted to examine the effects of varying the cloud characteristics on ice accretion on tower legs and on the aerodynamic coefficients around the ice-covered legs. First, the variations of droplet size distribution (DSD) and liquid water content (LWC) in vertical and streamwise directions were measured. Then, variations of ice accretion on an angle bar in the same direction as the flow were measured to determine the aerodynamic forces on a tower leg as a function of ice accretion. The ice accretion experiments were carried out under two conditions with different LWCs and air velocities. The drag coefficient was calculated with different masses and ice shapes for the angle bar as obtained in the experiments. The results showed a reduction in the drag coefficient in the vertical direction with increased local LWC and thicker ice accumulation.

*Keywords: Atmospheric icing, Cloud characteristics, aerodynamic coefficients, Liquid water content, angle bar drag coefficient.*

## 1. Introduction

Atmospheric icing can cause serious damages to power network equipment in cold climate regions. One of the most significant sources leading to such damages is the variation of the aerodynamic forces on the transmission line towers due to the combination of ice and wind loads. Meteorological parameters such as LWC and DSD are decisive factors in determining the various types of atmospheric ice accretion.

One of the important differences between natural aerosol clouds and its experimental models is their dimensions in relation to a size of the icing structures that are exposed to those clouds. The dimensions of the supercooled aerosol clouds are greater in all directions under natural icing conditions (Cober et al. 2001; Jeck 1996; Politovich 1989) whereas the same order of magnitude is observed for the same factors when simulating ice accretion in wind tunnel. Therefore, knowing the zone of the uniformity of the artificial aerosol clouds is essential in order to predict the local LWC and DSD. Although the dimensions of zone of uniformity of natural aerosol clouds are not achievable in experimental modeling, but it is possible to obtain LWC and DSD around the same level as appear in natural aerosol clouds. Different combinations of these characteristics produce different types of natural icing phenomena. The LWC is in the range of a few tenth of  $\text{g/m}^3$  under in-cloud icing conditions; however, values between 1 and  $10 \text{ g/m}^3$  were also observed under other ambient conditions such as freezing drizzle or freezing rain (Air Force Geophysics Laboratory 1985; Cober et al. 2001; Frisch et al. 2000; Jeck 1996; Jeck 2002). The droplet size falls in the range of a few  $\mu\text{m}$  to about  $50 \mu\text{m}$  under in-cloud icing conditions, whereas it takes significantly greater values under freezing drizzle (in the range of  $100 \mu\text{m}$ ) and

freezing rain (from the range of 100  $\mu\text{m}$  to several mm) conditions (Air Force Geophysics Laboratory 1985; Jeck 1996; Jeck 2002).

The LWC and DSD vary inside the aerosol cloud. These variations are more significant when the air velocity is low and when the cloud droplets are large. The main reason of these variations is related to gravity and inertia forces acting on supercooled droplets. These forces alter the trajectories of particles that contribute to the ice accretion (Kollar and Farzaneh 2007; Kollar and Farzaneh 2009). Thus, they have an influence on the ice mass and ice shape, resulting in varying aerodynamic coefficients on the tower.

The effects of ice accretion on the aerodynamics of a body have been studied for decades. Large-droplet ice accretion on aircraft wings is important to aircraft industry since its effects are crucial on aerodynamics. Bragg (1988) studied these effects on drag coefficient, lift coefficient and pitching moment that vary during aircraft control. The results showed that a ridge of ice aft of the boot can lead to large losses in lift, increase in drag and changes in the pitching moments. He continued this study with Lee (2003) to simulate the effects of large-droplet ice shapes on airfoil aerodynamics experimentally. They investigated the influence of simulated supercooled large-droplet ice accretion on a modified NACA 23012 airfoil. They realized that when the simulated ice was placed at critical chordwise locations, separation bubbles formed downstream of the simulated ice shape, and there was a dramatic reduction in the maximum lift coefficient which was then as low as 0.27.

For airfoil NLF0414, Bragg and Loth (2000) investigated the effect of simulated ridge ice shapes. They developed a computational program for higher Reynolds numbers to measure lift coefficient, calculating that the maximum lift coefficient for this airfoil was 0.68. They investigated various simulated ice shape sizes and geometries, and concluded that the variation in the simulated ice shape geometry had only minor effects on the airfoil aerodynamics.

Lynch and Khodadoust (2001) provided a comprehensive review on the effects of ice accretion on aircraft aerodynamics. They listed a number of experimental measurements for various forms of icing such as in-flight and ground ice accretion. The reviewed in-flight icing categories include initial and inter-cycle ice accretion, runback/ridge ice accretion for large water droplet, and rime and glaze ice accretion including ice shapes. Vargas et al (2002) and Vargas (2005) studied and simulated different formations of ice accretions on swept wings in natural icing conditions.

Whereas all these studies concerned characteristics of aerodynamic bodies, another category named bluff bodies was also investigated by Yeo and Jones (2011). They studied the flow around a circular cylinder with low aspect ratio using eddy simulation. They showed that three dimensional flows and the associated force on a yawed and inclined cylinder were significantly influenced by the spanwise aspect ratios and spanwise boundary conditions. Cheng and Wang (2013) simulated the flow field around spherical hailstones of different size and provided empirical relations to calculate the drag coefficient as a function of hail diameter.

The investigations mentioned above studied the effects of different types of ice accretion separately. Furthermore, most of them used aerodynamic airfoils as samples. However, studying

the bluff bodies is a significant aspect of icing phenomena. Therefore, it is important to consider the effects of meteorological parameters on ice accretion as well as the aerodynamic performance for such bluff bodies, such as tower legs, which is of interest to this study. Its main goal is to study the effects of streamwise and vertical variations of cloud characteristics on ice accretion on tower legs and on the aerodynamic coefficients around tower legs with ice. In order to achieve this goal, first the streamwise and vertical variations of cloud characteristics, namely its LWC and droplet size, were measured in the test section of a horizontal icing wind tunnel. The results obtained in this preliminary study were published in Banitalebi Dehkordi et al. (2011). Then, further measurements were made to study how these variations influence (i) the mass and shape of the ice accumulated on a simple angle bar (reduced model of tower leg), and (ii) the aerodynamic coefficients around the ice-covered angle bar.

## **2. Experimental Set-up**

### **2.1. Apparatus**

Experimental data were collected in the CIGELE atmospheric icing research wind tunnel (CAIRWT). The CAIRWT is a vertical closed-loop, low-speed icing wind tunnel 30 m in length, including a 3-m-long test section whose rectangular cross section measures 0.46 m in height and 0.92 m in width. The maximum velocity in the test section is 28 m/s measured with an accuracy of  $\pm 1\%$  and both longitudinal and transverse turbulence levels are less than 1 %. An accepted standard technique is used at CAIRWT to simulate atmospheric icing processes, which involves injecting water at room temperature into a cold air stream through air-assisted nozzles located at the trailing edge of a horizontal spray bar.

### **2.2. DSD and LWC measurements**

LWC and DSD were measured using an integrated system for icing studies, manufactured by Droplet Measurement Technologies. This instrument has two probes for droplet size measurement, the Cloud Imaging Probe (CIP) and the Cloud Droplet Probe (CDP), whose operation is based on optical imaging techniques. The CDP is designed to measure particles with diameters between 3  $\mu\text{m}$  and 50  $\mu\text{m}$ , whereas the CIP measures particles ranging in size from 25  $\mu\text{m}$  to 1550  $\mu\text{m}$ . The CIP is a combination probe incorporating several basic measuring instruments to characterize cloud parameters, also including a hot-wire LWC sensor, an air temperature sensor and a Pitot tube air speed sensor. The measured data are displayed by the particle analysis and collection system (PACS) which has an intuitive graphical user interface at the host computer and provides powerful control of the measured parameters while simultaneously displaying real-time size distributions and derived parameters.

The integrated system described above was used in different vertical and streamwise positions in the tunnel test section for different free-stream velocities and initial DSDs (DSD at nozzle outlet). Throughout the tests, the temperature was set at 15°C and the duration of each measurement was 30 s. The measurements were done for four air velocities;  $V_a = 5, 10, 20,$  and 28 m/s. The pressures in the nozzle air and water lines in the wind tunnel determine the DSD and LWC in the produced spray. The water pressure,  $p_w$ , was set at 450 kPa, and the air pressure,  $p_a$ , was varied from 180 kPa to 620 kPa. Thereby aerosol clouds were produced with varying DSD and LWC so that they simulated different icing conditions including in-cloud icing, freezing

drizzle and freezing rain. The upper limit for air pressure was determined by the condition that the nozzle could produce spray. Further increase of air pressure above 620 kPa with unchanging water pressure would block the water in the nozzle mixing chamber so that spray was not produced. These measurements were repeated for three vertical positions with 0.07 m increments and four horizontal positions with 0.5 m increments. The adopted co-ordinate system was as follows:

- The origin was at the center point of the test section.
- The x-axis was coincident with the tunnel longitudinal centre line and it was oriented in the direction of the free-stream velocity. Its zero was coincident with the position of the angle bars to be tested.
- The y-axis was placed vertically and oriented upward.

Thus, measurements were made at the following positions:  $x = -1, -0.5, 0, +0.5$  m;  $y = -0.07, 0, +0.07$  m.

### 2.3. Ice Accretion Measurements on Tower-Leg Model

Two angle bars fabricated from AL 6061-T6 with length of 0.92 m and 0.46 m and the same cross section of 5.1 cm  $\times$  5.1 cm  $\times$  0.64 cm (2 in  $\times$  2 in  $\times$  0.25 in) were used in the ice accretion tests. They were the reduced models of real tower legs, which fit into the tunnel test section.

The 0.92-m-long angle bar was mounted in the test section horizontally in three vertical positions  $y = -0.07, 0, +0.07$  m and in three streamwise positions,  $x = -0.5, 0, +0.5$  m for the ice accumulation tests. The 0.46 m angle bar was used vertically in the same three streamwise positions. Table 1 shows precipitation types of different icing conditions which were considered in the ice accretion tests.

Table 1, Precipitation types of ice accretion measurements

Icing Conditions	Precipitation type	$V_a$ (m/s)	$p_w$ (kPa)	$p_a$ (kPa)	$T_a$ (°C)	t(min)
I	Freezing drizzle	25	300	300	-5	30
II	Freezing rain	12	300	200	-5	30

It should be noted that in-cloud icing conditions were not simulated in these experiments because the accumulation of sufficient amount of ice with low LWC would take excessively long time. The following data were collected after each experiment, using the collection method presented in Kollar and Farzaneh (2010): mass of ice accretion per unit length of angle bar, ice shape, and profile of ice accretion were measured. Ice shapes were recorded by taking photos of their front and top views. In order to measure ice mass, the tower-leg model was taken off its supports and set into a specially designed support for further examination outside the tunnel. A thin preheated aluminium cutter was used to cut the ice specimens for measuring their mass and length. Samples with different lengths were taken from different parts of the angle bar. After cutting the ice accretion, additional photos were taken to record ice profiles.

## 3. Results and discussion

### 3.1. Streamwise and Vertical Variations of Median Volume Diameter (MVD) and LWC of the droplets

The effects of air velocity and nozzle pressures on DSD in the produced spray and on the LWC in the cloud in the middle of test section of a low-speed horizontal wind tunnel were studied in Kollar and Farzaneh (2009) and in Kollar et al. (2006), respectively. Different parameters influencing LWC were discussed in details in Kollar and Farzaneh (2009). The effects of temperature on droplet size were studied in Kollar et al. (2006), and they obtained that temperature variation resulted only in a few percent change in the MVD. Therefore, the temperature was kept constant at 15°C in the DSD and LWC measurements in the present study. The streamwise and vertical variations of these characteristics in the test section were discussed in Kollar and Farzaneh (2011) for two specific icing conditions. The following discussion focuses on the streamwise and vertical variations of MVD and LWC for different air velocities and nozzle pressures.

As described in Section “Ice accretion Measurements on Tower-Leg Model”, experiments were carried out in 4 streamwise and 3 vertical positions, and for 4 air velocities. Furthermore, 6 different nozzle air pressures were applied between 180 and 620 kPa, when the nozzle water pressure was kept constant. In order to reduce the number of figures, variations along the streamwise directions are presented at one vertical position only, and variations along the vertical direction are shown at one streamwise position only. The MVD and LWC are drawn in the figures of this section as functions of differential pressure,  $dp = p_w - p_a$ , which is a key parameter in determining DSD and LWC (Kollar and Farzaneh 2009). An additional parameter, either the streamwise or the vertical position, is varied in each figure.

Fig. 1 presents the MVD variations along the streamwise direction at  $y = -0.07$  m. The MVD is approximately constant for the lowest differential pressures. It then increases until reaching a maximum which is followed by a decreasing tendency. The value of differential pressure where the increasing tendency begins increases with air velocity (from about  $-100$  kPa for 5 m/s to about  $+50$  kPa for 28 m/s). The maximum also appears for higher differential pressure when the air velocity is higher: it is around 100-150 kPa for 5 m/s, around 200 kPa for 10 m/s, and out of diagram for 20 and 28 m/s (above 300 kPa). The gravity effect is more significant than the drag effect for low air velocity. Hence, the MVD at a specific height decreases along the streamwise direction, because the larger droplets go toward the bottom of test section. When the velocity increases, the drag effect becomes more significant than the gravity effect for clouds including small droplets only, and droplet separation according to their size occurs only for clouds with the larger droplets. Correspondingly, the curves presenting MVDs at different streamwise positions become distinguishable for aerosol clouds with MVD of  $20 \mu\text{m}$  when air velocity is the lowest (5 m/s), whereas this limit increases to about  $50 \mu\text{m}$  when air velocity is the highest (28 m/s). Similar tendencies were observed at the vertical position  $y = 0$  m with smaller differences between MVDs at different streamwise positions. These differences vanish nearly completely at  $y = +0.07$  m, because this position is close to the top of cloud where droplets are small even at the streamwise position of  $x = -1$  m.

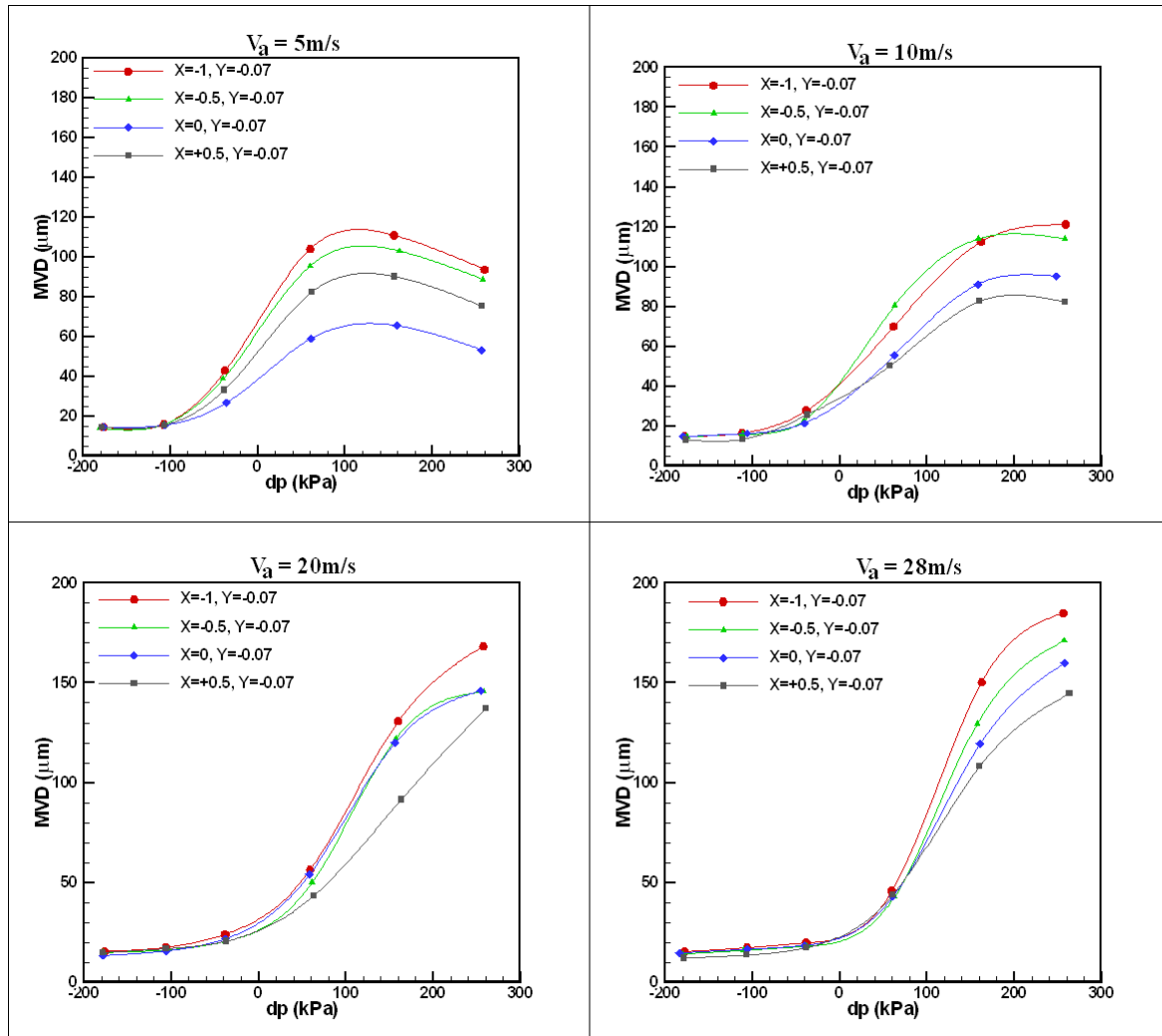


Fig. 1, MVD variations along the streamwise direction at  $y = -0.07 \text{ m}$

LWC increases with the differential pressure even for smaller differential pressures until reaching a maximum which then is followed by a decreasing tendency (see Fig. 2). Similarly to the MVD, a maximum for LWC also occurs at higher differential pressure when the air velocity is higher. LWC at the height of  $y = -0.07 \text{ m}$  decreases in the streamwise direction at 5 m/s; this tendency is the same at 10 m/s, but the curves obtained for different streamwise positions appear closer to each other; and LWC becomes constant along the streamwise direction when the air velocity approaches 20 m/s. LWC does not change significantly in the streamwise direction at 20 m/s, but it is greater for downstream positions for some differential pressures; and the tendency is reversed completely at 28 m/s, i.e. the LWC at the height of  $y = -0.07 \text{ m}$  increases in the streamwise direction. This behavior may be explained by the fact that when air velocity is high, the cloud is not much extended vertically at the beginning of the test section, but more and more droplets reach the vertical position of  $y = -0.07 \text{ m}$  as they move forward in the test section. This explanation is also confirmed by the fact that a similar reverse tendency was not observed at  $y = 0 \text{ m}$ . Most of the cloud was around mid-height at the beginning of the test section for all the air velocities considered, so that LWC at this height did not increase in the streamwise direction. The LWC was significantly lower at the height of  $y = +0.07 \text{ m}$ , and variation in the streamwise

direction was small. However, it is more difficult to evaluate the tendency, because this position is very close to the boundary of the cloud.

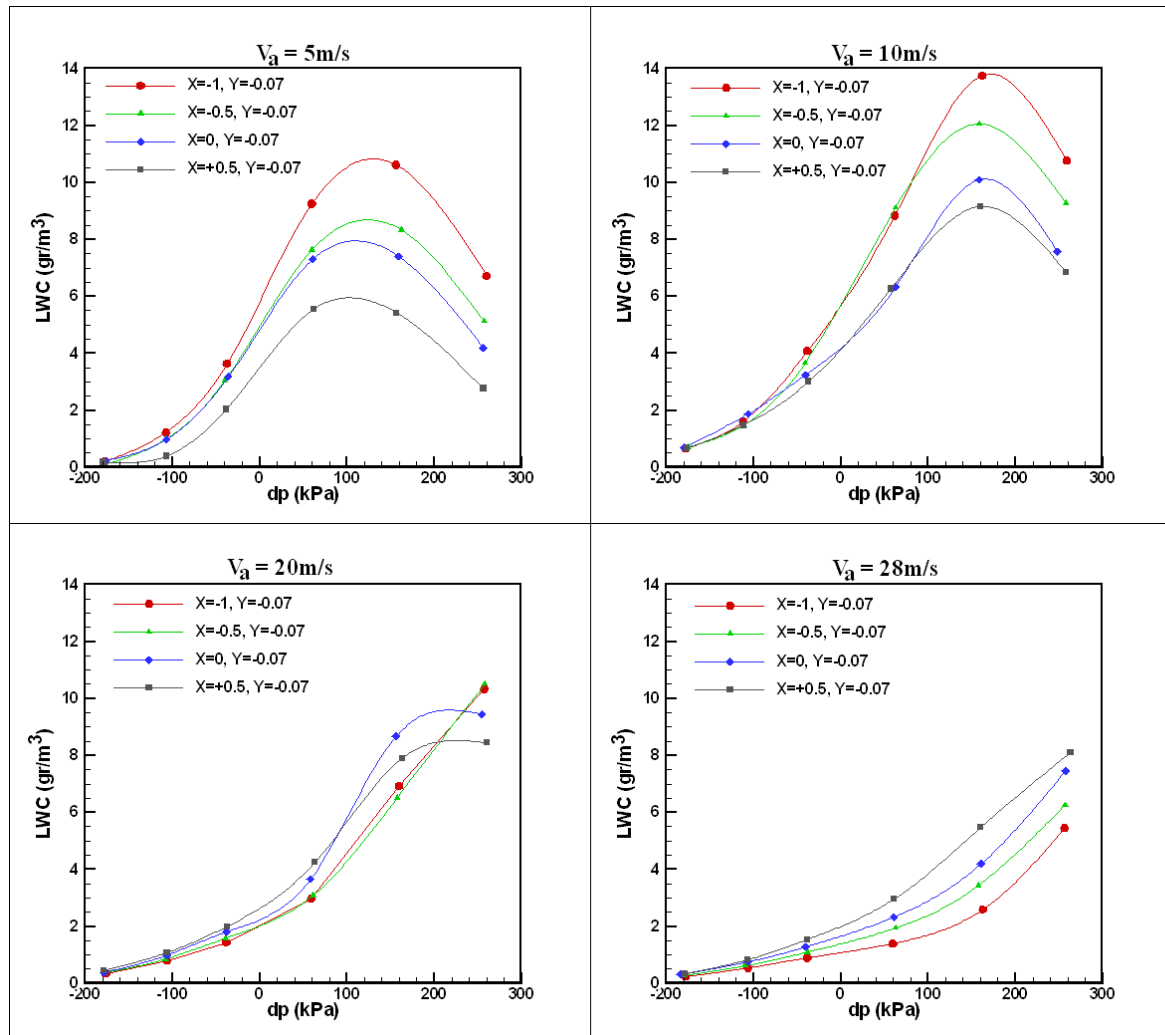


Fig. 2, LWC variations along the streamwise direction at  $y = -0.07 \text{ m}$

Figure 3 presents the variation of MVD in the vertical direction at the streamwise position of  $x = 0.5 \text{ m}$ . MVD increases from top to bottom for high enough differential pressures, i.e. when clouds with MVD of at least  $20 \mu\text{m}$  are produced, for air velocity of  $5 \text{ m/s}$ . For higher air velocities, MVD was similar or even greater at mid-height ( $y = 0 \text{ m}$ ) than at the vertical position of  $y = -0.07 \text{ m}$  for clouds with MVDs up to about  $80 \mu\text{m}$ . Then, when the cloud included larger droplets, the greatest MVD value was measured close to the bottom of the cloud (at  $y = -0.07 \text{ m}$ ). The larger droplets tend to move toward the bottom of the tunnel during their flow in the test section. However, when the droplets are not large enough ( $\leq 80 \mu\text{m}$ ) and the air velocity is high enough ( $\geq 10 \text{ m/s}$ ), then numerous large droplets are still found close to mid-height at the streamwise position of  $x = 0.5 \text{ m}$ .

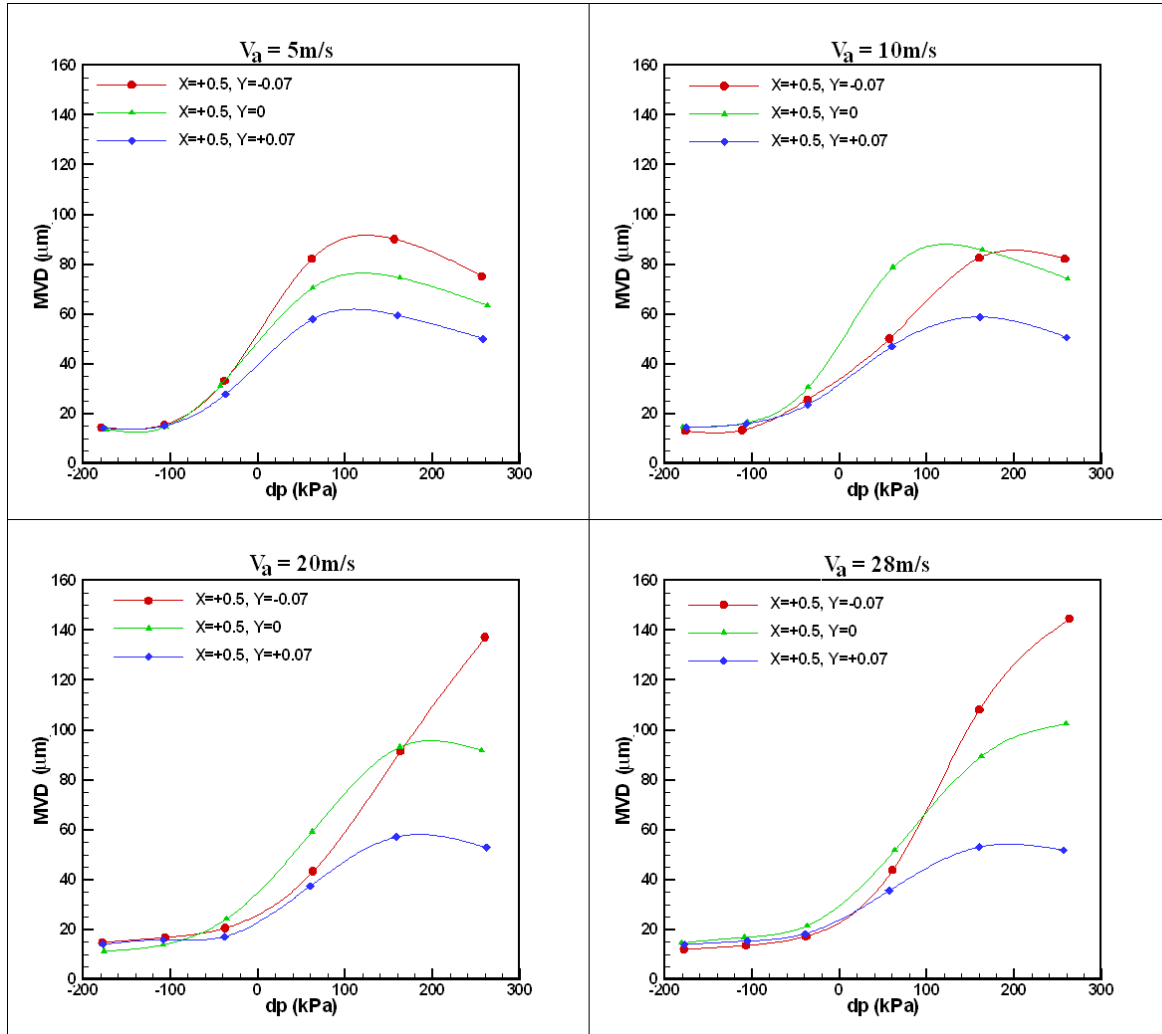


Fig. 3, MVD variations along the vertical direction at  $x = 0.5$  m

The LWC also increases in the vertical direction toward the bottom for low air velocities and if the MVD of the cloud is large enough the LWC increases too for higher air velocities. When the differential pressure is small, and consequently the droplets are not too big ( $MVD \leq 80 \mu\text{m}$ ), the LWC at the vertical position  $y = 0$  cm is equal or greater than at  $y = -0.07$  m at the streamwise position  $x = 0.5$  m as shown in Fig. 4. This is due to the same process that explained the same tendency for MVD in the previous paragraph. Upstream from this position, i.e. for  $x = -1, -0.5$ , and  $0$  m where the aerosol cloud is less expanded, for the higher air velocities considered (20 and 28 m/s), and for clouds without large droplets, LWC is significantly greater at mid-height ( $y = 0$  m) than at the bottom of the cloud ( $y = -0.07$  m). The smallest LWC value is at the top of the cloud ( $y = -0.07$  m) for all the cases considered.

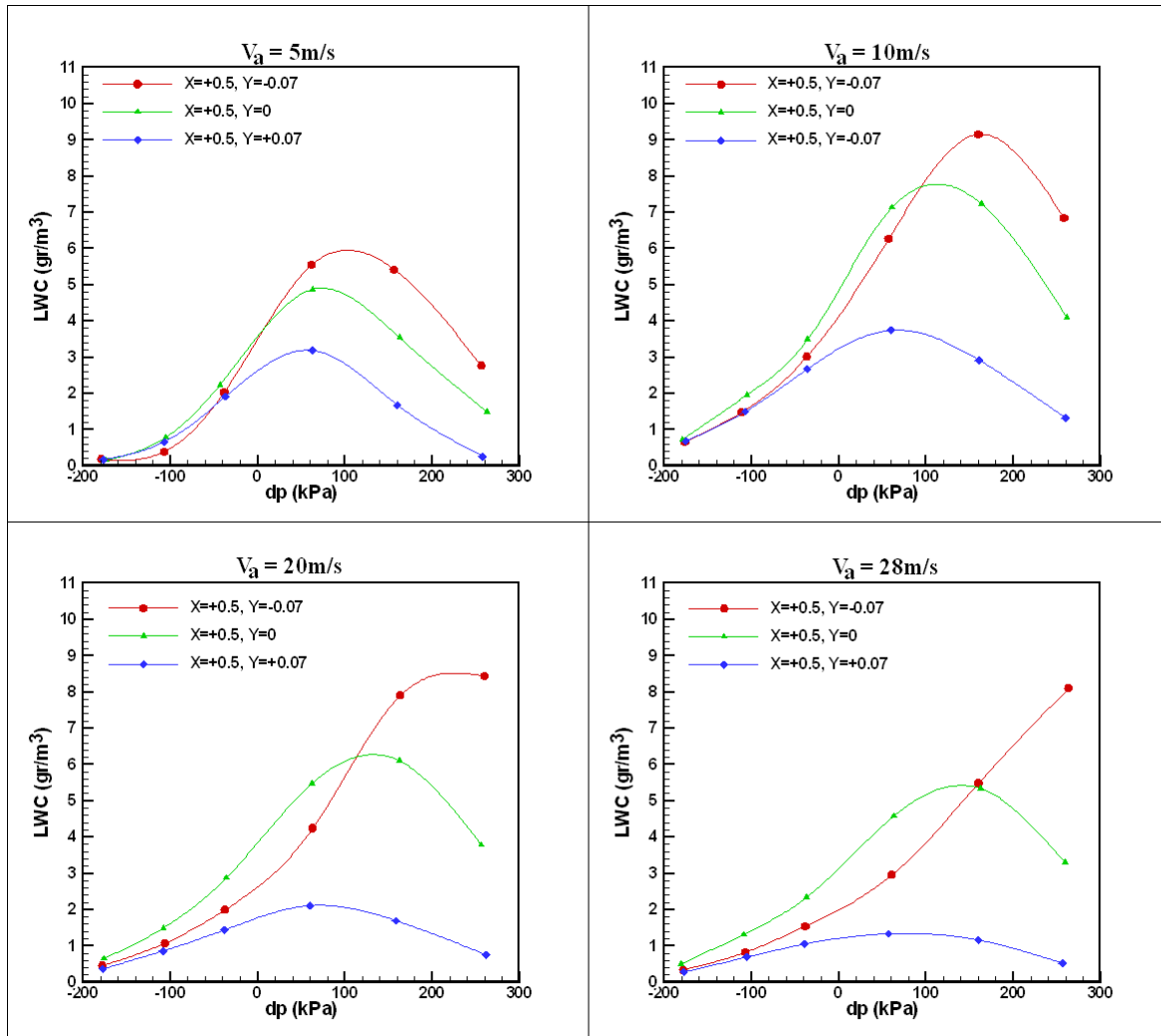


Fig. 4, LWC variations along the vertical direction at  $x = 0.5$  m

### 3.2. Streamwise and Vertical Variations of Ice Accretion on Angle Bar

The previous section discussed the streamwise and vertical variations of MVD and LWC for different air velocities and nozzle pressures. The present section mainly focuses on studying variations of ice accretion on an angle bar in streamwise and vertical directions under two types of icing conditions. Table 2 shows again thermo-physical parameters of two icing conditions with their LWC and MVD. In order to reduce the number of figures, variations along the streamwise and vertical directions under the same condition and from the same view are presented in one figure.

Table 2, Thermo-physical parameters for icing conditions

Icing Conditions	Temperature (°C)	Velocity (m/s)	Air pressure (kPa)	Water Pressure (kPa)	LWC (center of test section) (gr/m <sup>3</sup> )	MVD (center of test section) (μm)
I	-5	25	300	300	2.8	39
II	-5	12	200	300	5.8	84

The variation in the ice mass per unit length is shown in Fig. 5 for three vertical positions:  $y = +0.07$ ,  $0$ , and  $-0.07$  m. The ice mass in the middle of angle bar increases in the streamwise direction below mid-height ( $y = -0.07$  m), which is a consequence of increasing LWC in the same direction at this height for the higher velocities considered, as can be seen in Fig. 2. The ice profiles on the angle bar for  $y = -0.07$  m also show that the number of impinging droplets increase downstream in the test section (Fig. 6). Ice accretion at the position  $y = +0.07$  m does not show an increasing or decreasing tendency, which may be consequential to the fact that this position is close to the cloud boundary that may oscillate in an interval of a few cm. Thus, LWC can considerably change even in a short vertical interval and it may also vary in time at the same vertical position (Kollar and Farzaneh 2011), which makes the tendencies difficult to measure. As the cloud is less expanded in the vertical direction for high velocities, the highest ice masses were measured at mid-height ( $y = 0$  m), which corresponds to the highest LWCs at mid-height (Fig. 4).

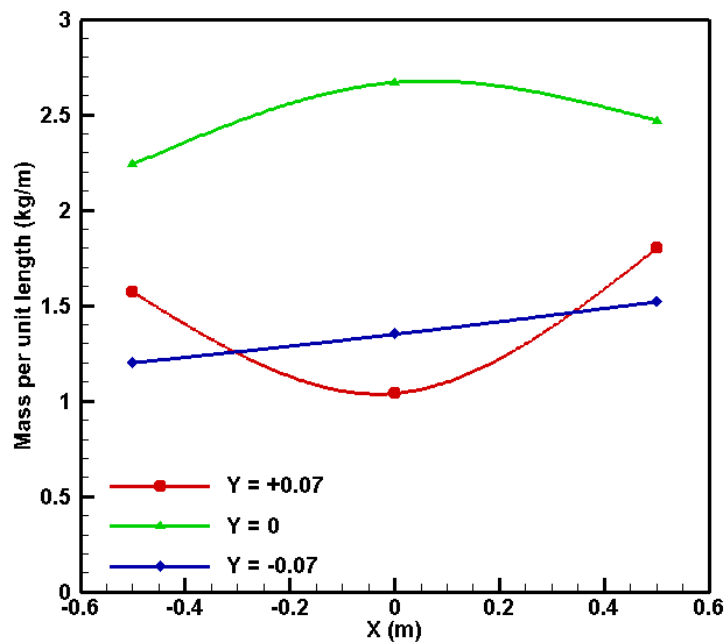


Fig. 5, Mass per unit length,  $P_w=300$  kPa,  $P_a= 300$  kPa and  $V_a= 25$  m/s

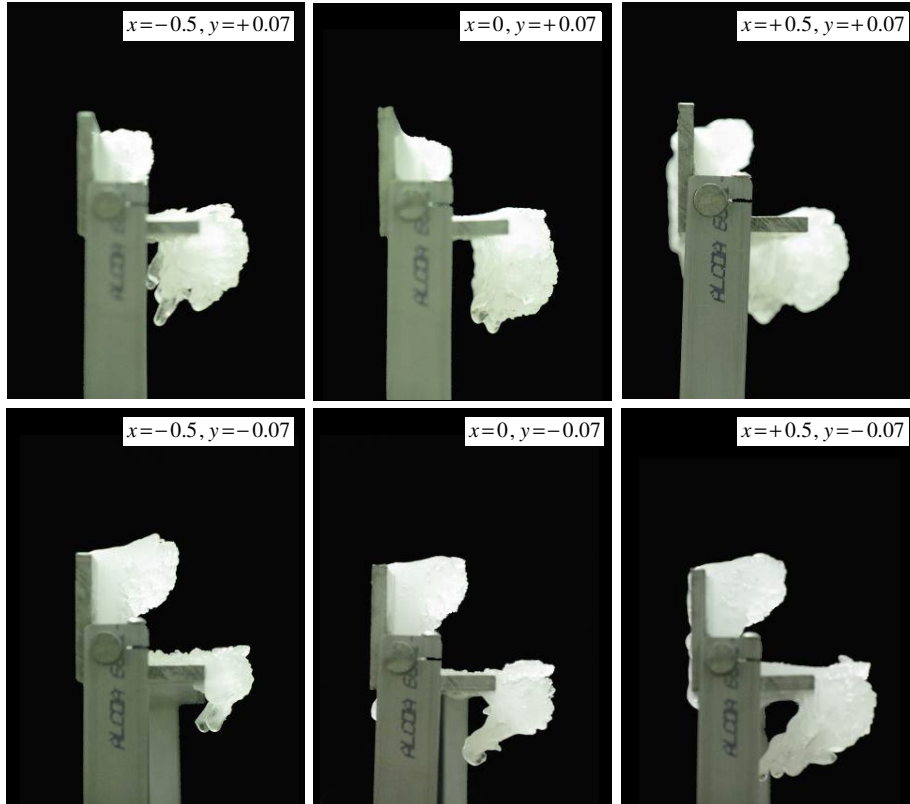


Fig. 6 Side view of the iced horizontal angle bar,  $P_w=300$  kPa,  $P_a= 300$  kPa

According to the front views shown in Fig. 7, the amount of accreted ice for  $x = 0$ ,  $y = +0.07$  is lower in the middle of the angle bar and it increases slowly towards its sides. This non-uniformity is probably due to the cloud boundary as discussed in the previous paragraph. Correspondingly, the accreted ice becomes more uniform toward the bottom of the test section.

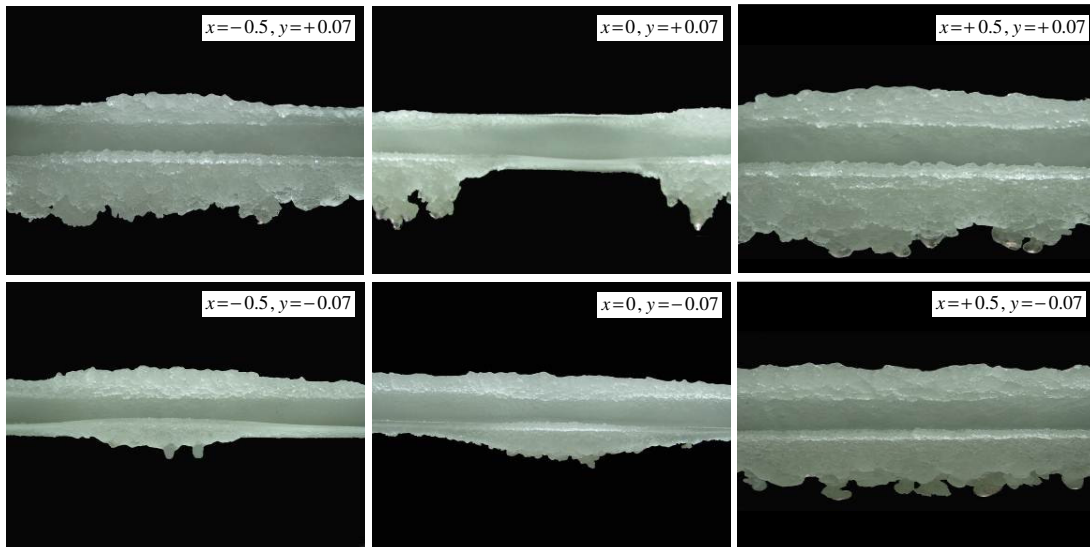


Fig. 7 Front view of the iced horizontal angle bar,  $P_w=300$  kPa,  $P_a= 300$  kPa

The top views in Fig. 8 also show that the ice accretion is more uniform for  $y = -0.07$  m than for  $y = +0.07$  m. However, there is a curved shape at all positions which correspond to the transverse distribution of LWC in the test section (Banitalebi Dehkordi H. et al. 2011).

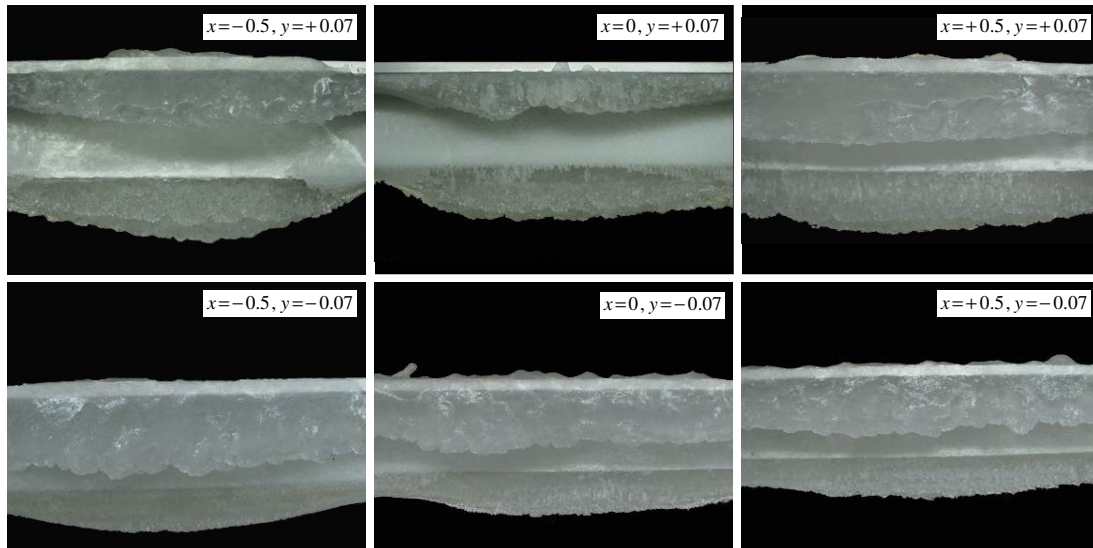


Fig. 8 Top view of the iced horizontal angle bar,  $P_w=300$  kPa,  $P_a= 300$  kPa

For the condition with lower velocity, the variation in the ice mass per unit length is shown in Fig. 9 for two vertical positions:  $y = +0.07$  m and  $-0.07$  m. The tendency of LWC to increase in the streamwise direction for high velocities at  $y = -0.07$  m changes to a decreasing tendency for low velocities as seen in Fig. 2. Correspondingly, the mass per unit length of accretion decreases in the streamwise direction. Similarly to the case with higher velocity, a clear tendency cannot be seen at  $y = +0.07$  m. However, the accretion maximum moves from mid-height toward the bottom of the tunnel. More and more droplets tend to move towards the bottom of test section, because the effect of gravity on droplet trajectories becomes more significant than that of inertia.

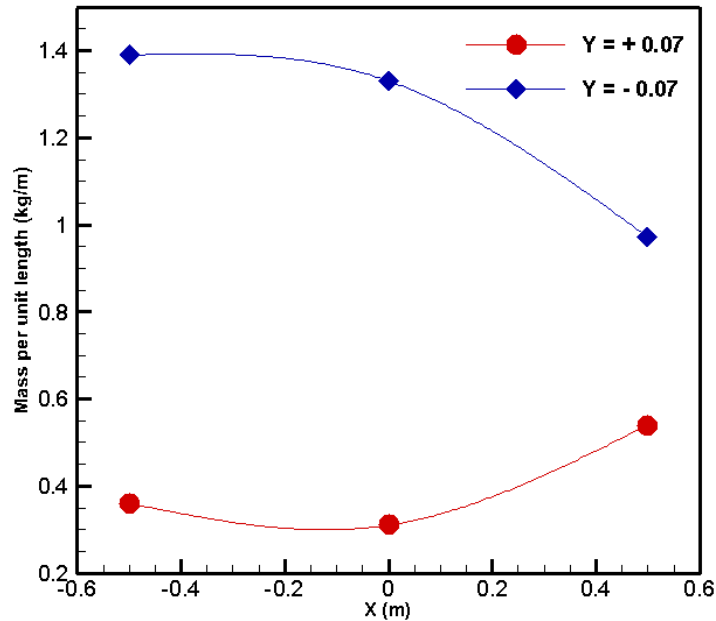


Fig. 9 Mass per unit length  $P_w=300$  kPa,  $P_a=200$  kPa and  $V_a=12$  m/s

According to Fig. 10, the streamwise variation of accreted ice for the lower velocity at  $y = +0.07$  m is similar to that for the higher velocity (see Fig. 7), and has a minimum value at the middle of the test section. It means that the tendency of the mass per unit length is the same at  $y = +0.07$  m for the two velocities,  $V_a=12$  m/s and  $V_a=25$  m/s. However for  $y = -0.07$  m, the mass per unit length has an increasing tendency for  $V_a=25$  m/s, and a decreasing tendency for  $V_a=12$  m/s. Icicles in Figs. 10 and 11 also show that the cloud extends toward the bottom. Icicles grow rapidly at  $y = -0.07$  m whereas those close to the top boundary of the cloud (i.e. at  $y = +0.07$  m) are significantly shorter (except a few icicles at  $x = -0.5$  m position). Also, it is obvious from the top views (Figs. 8 and 12) that the accreted ice is more uniform for  $V_a=12$  m/s than for  $V_a=25$  m/s.

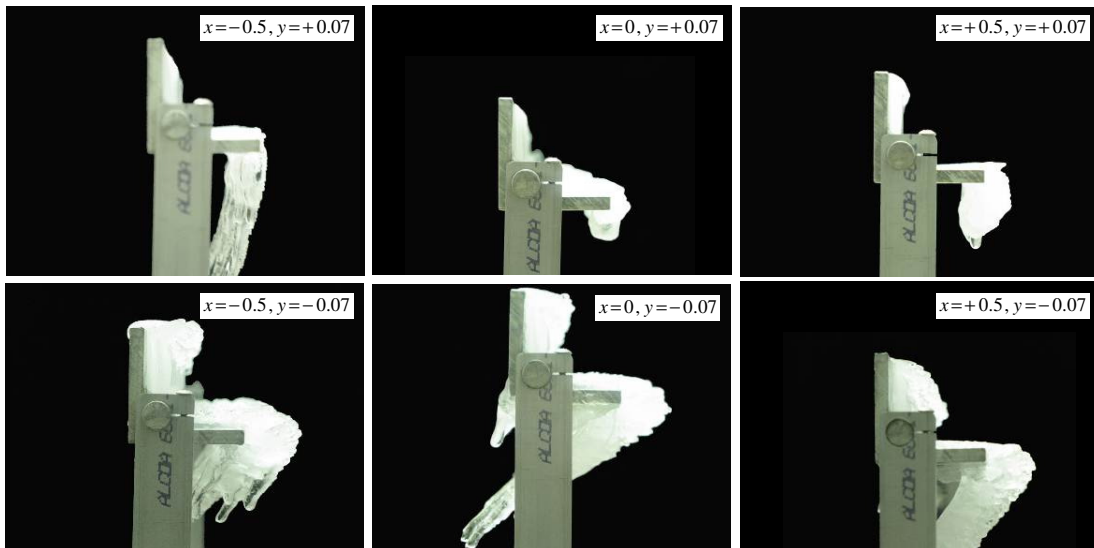


Fig. 10 Side view of the iced horizontal angle bar,  $P_w=300$  kPa,  $P_a=200$  kPa

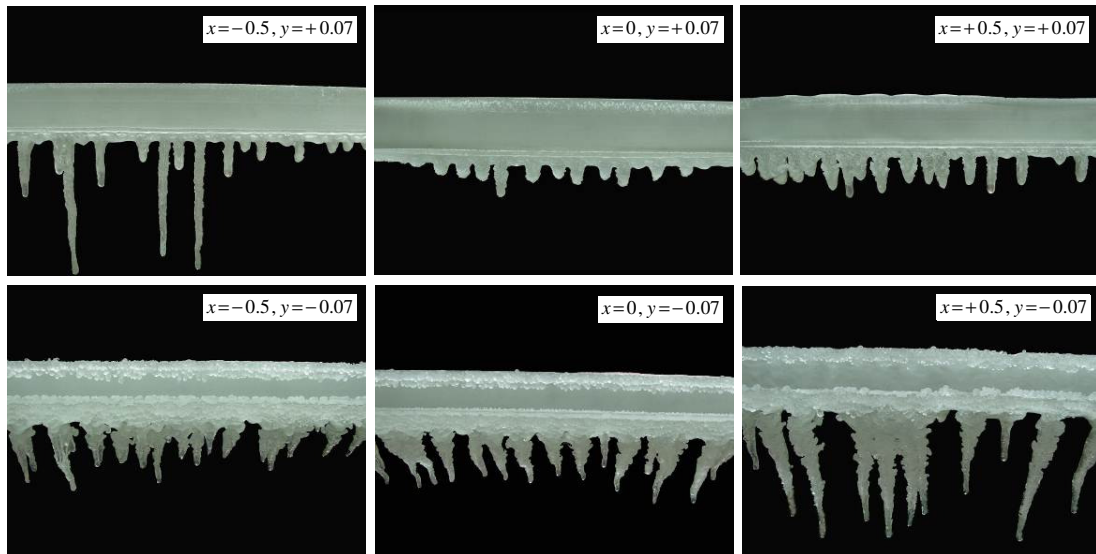


Fig. 11 Front view of the iced horizontal angle bar,  $P_w=300$  kPa,  $P_a= 200$  kPa

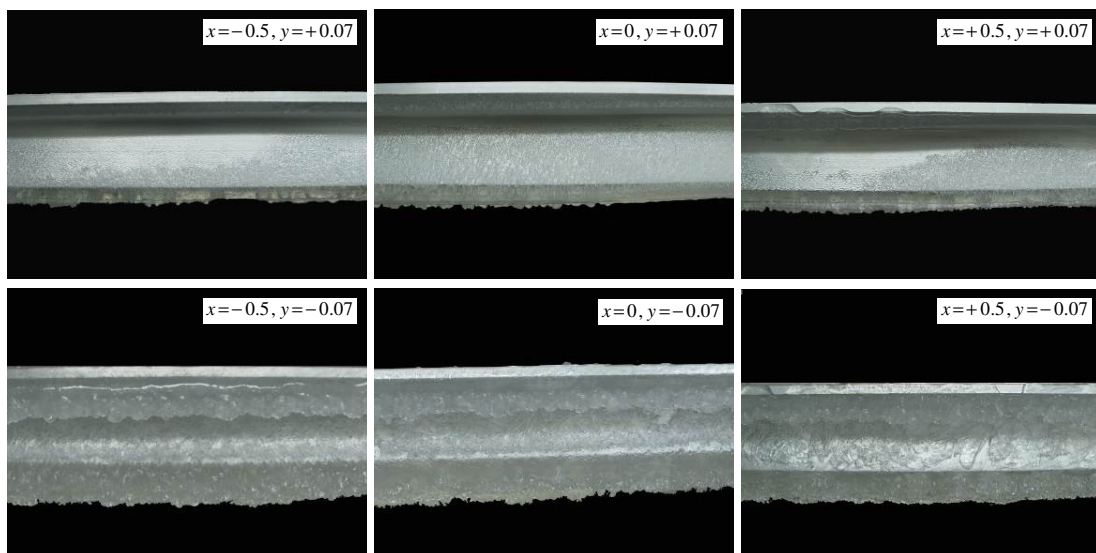


Fig 12. Top view of the iced horizontal angle bar,  $P_w=300$  kPa,  $P_a= 200$  kPa

Results of ice accretion tests on vertical angle bars are summarized in Figs. 13-15. These results provide a more detailed view of the vertical variation of ice mass, and they also make possible the comparison of clouds in their entire vertical dimension.

Figure 13 compares the ice mass per unit length for the two velocities considered. The variation of ice mass per unit length in the streamwise direction for the higher air velocity (25 m/s) is not more than the measurement error (the difference between the ice masses is approximately 4% at the  $x = -0.5$  m and  $x = +0.5$  m positions). However, the ice mass decreases considerably in the streamwise direction (about 40% between the same positions) for the lower air velocity (12 m/s). The ice shapes in Figs. 14 and 15 explain these tendencies.

Figure 14 shows that for high velocities the ice accretion has a maximum in the middle of the angle bar and that it decreases quickly upward and downward with no accretion on the top and

on the bottom. The entire cloud is in the middle part for both streamwise positions. It seems that the thickness of the accreted ice is a bit higher at the lower side of the angle bar (right hand side in Fig. 14), which is confirmed by the front view. However, the ice accretion then vanishes quickly from the bottom of the angle bar.

A comparison between Fig. 14 and Fig. 15 shows that for the lower velocity there is no maximum in the accretion shape as for the higher velocity, but that the amount of accreted ice increases toward the bottom, the accretion extending up to the bottom of the angle bar. Thus, the effect of gravity is more considerable for  $V_a = 12$  m/s.

An additional observation from Fig. 13 is that the accreted ice per unit length for  $V_a = 25$  m/s is higher than for  $V_a = 12$  m/s which is in agreement with the results of experiments with horizontal angle bars (cf. Figs. 5 and 9). The effects of three important factors on ice shape during ice accretion was observed: (i) effects of gravity force for low droplet velocity, (ii) effects of distance between spray bar with nozzles and the angle bar, (iii) effects of temperature on immediate freezing of impinging droplets influencing the shape of ice on the surface of the angle bar.

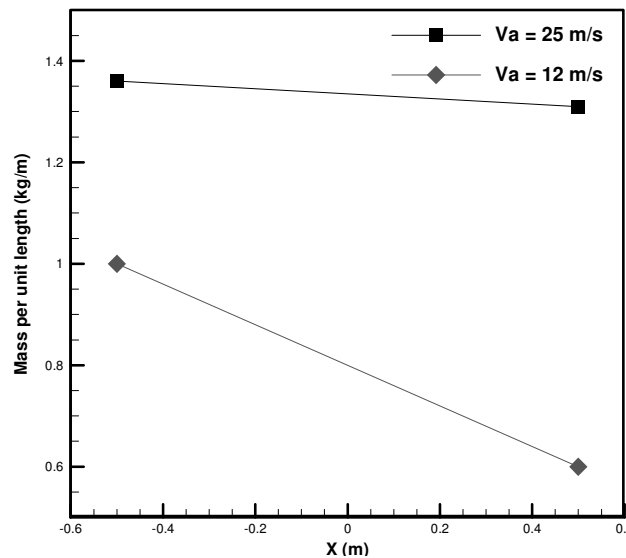


Fig. 13 Mass per unit length for  $V_a = 25$  m/s and  $V_a = 12$  m/s

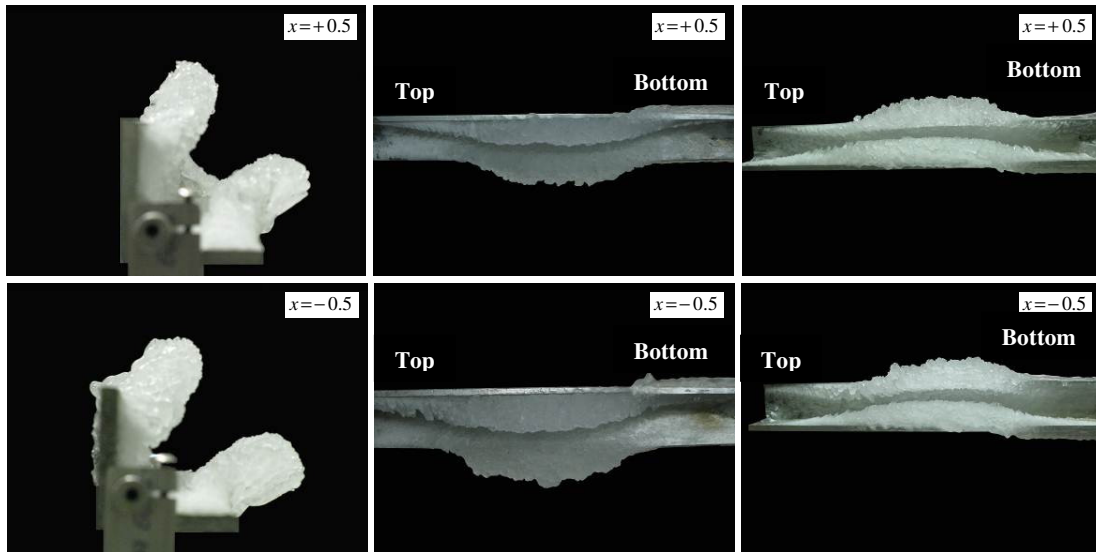


Fig. 14 Accreted vertical angle bar,  $V_a = 25$  m/s

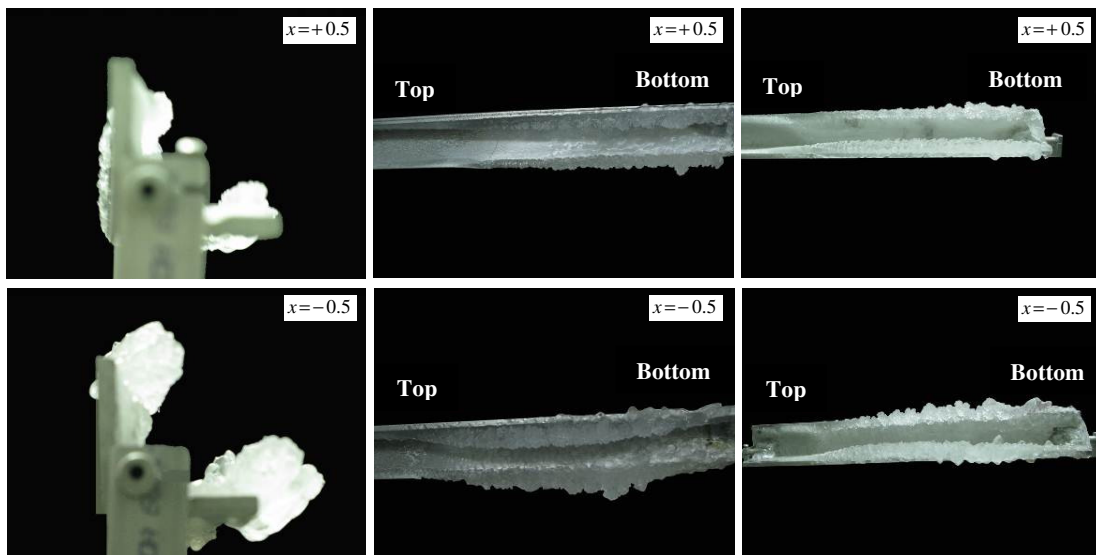


Fig. 15 Accreted vertical angle bar,  $V_a = 12$  m/s

### 3.3. Calculation of Drag Coefficients of Ice-Covered Angle Bars

An important practical question is to determine how the aerodynamic forces on a tower leg vary due to ice accretion. In particular, the drag coefficient is calculated for the angle bar with different mass and shape of ice accretion as obtained in the experiments described in the previous section. The procedure of calculation is based on the standard ISO12494 (2001). The calculation of drag coefficients for non-aerodynamic geometries such as an angle bar is difficult. The calculation requires several input parameters such as ice type, ice thickness, and drag coefficient of angle bar without ice.

In order to calculate drag coefficients of ice-covered angle bars, first, the type of ice must be specified which was glaze for these experiments. Considering this and the thickness of angle bar which was less than 0.3 m, the corresponding tables from the standard ISO12494 were selected.

Then, with the help of pictures of the experimentally accumulated ice on the angle bar, the category of glaze deposits, ICGx, was obtained from the above mentioned standard. The drag coefficient for the angle bar without ice ( $C_0$ ) was available in Hoerner (1965). Once these data were known, tabulated data from the same standard provided the drag coefficient of the ice-covered angle bar.

The drag coefficient for the lower liquid water content and higher air velocity was calculated to be about 1.63 for the  $y = +0.07$  m and  $x = -0.5, 0, +0.5$  m position whereas it was calculated to 1.59 for the  $y = -0.07$  m and  $x = -0.5, 0, +0.5$  m position. In other words, the drag coefficient was found to vary vertically, but to be independent from the streamwise position (see Table 2).

Table 2. Drag coefficient variation for iced angle bar in vertical position (lower LWC and higher velocity)

LWC ( $\text{g/m}^3$ )	$V_a$ (m/s)	$C_0^*$	$C_i^{**}$	y (m)
2.8	25	1.75	1.63	+ 0.07
2.8	25	1.75	1.59	-0.07

\*  $C_0$ : drag coefficient without ice

\*\*  $C_i$ : drag coefficient with ice

The drag coefficient for an angle bar with higher liquid water content and lower air velocity was calculated to be about 1.75 for  $y = +0.07$  m and  $x = -0.5, 0, +0.5$  m which was same as the drag coefficient for the angle bar without ice. It was observed that the ice thickness was less than 10 mm at this vertical position. The drag coefficient for the  $y = -0.07$  m and  $x = -0.5, 0, +0.5$  m position was calculated to be about 1.61. The results show that for the lower velocity the ice effects for  $y = -0.07$  m are more important than for  $y = +0.07$  m, as shown in Table 3.

Table 3. Drag coefficient variation for iced angle bar in vertical position (higher LWC and lower air velocity)

LWC ( $\text{g/m}^3$ )	$V_a$ (m/s)	$C_0$	$C_i$	y (m)
5.8	12	1.75	1.75	+ 0.07
5.8	12	1.75	1.61	-0.07

For the vertical angle bar it was complicated to calculate the drag coefficient. For Standard ISO12494, one of the assumptions is that the ice accumulated on the model is uniform. For a vertical angle bar, however, the effect of gravity changes the shape of the ice along the bar. Therefore, the recommendation for estimating drag coefficient of such non-uniformly iced angle bars, or tower legs, is to divide the angle bar into smaller pieces for which ice thickness may be assumed constant, and to determine the drag coefficient as a function of the position along the bar. Instead of this procedure, since experiments were also carried out on horizontal angle bars at different vertical positions, these tests were used here to obtain an approximation as to how the drag coefficient varies vertically.

## 4. Conclusion

Two series of experiments were carried out: (i) DSD and LWC measurements in order to obtain the streamwise and vertical variations of these parameters in an aerosol cloud; and (ii) ice accretion measurements on an angle bar in order to obtain streamwise and vertical variations of ice mass and shape. Then, a methodology was applied to determine the drag coefficient of the angle bar with ice and its dependence on its position in the cloud.

It was found that the gravity effect on droplet trajectories is more significant than the drag effect for low air velocity, which can be observed on the variation of MVD and LWC in both

streamwise and vertical directions because the larger droplets tend to go toward the bottom of test section. When the velocity increases, the drag effect becomes more significant than the gravity effect for clouds including small droplets only, and droplet separation according to their size occurs only for clouds with the larger droplets.

The larger droplets move toward the bottom of the tunnel during their flow in the test section. However, when the droplets are not large enough (less than about 80  $\mu\text{m}$ ) and the air velocity is high enough (greater than 10 m/s), then numerous large droplets are still present close to mid-height even at the streamwise position of  $x=0.5$  m leading to the greatest MVD and LWC at mid-height. The LWC increases in the vertical direction toward the bottom for low air velocities and if the MVD of the cloud is large enough then also for higher air velocities. Results of ice accretion measurements on the angle bar reflect the observation that ice tends to accumulate mostly in positions where LWC is higher.

The effect of accreted ice has also been observed on the drag coefficient. The drag coefficient of the horizontal angle bar may change by 5-10% due to ice accretion. For the vertical angle bar it was complicated to calculate drag coefficient. For Standard ISO12494 one of the assumptions is the ice accumulated on the model is uniform. For a vertical angle bar, however, the gravity effect changes the shape of the ice along the bar. Therefore, to estimate the drag coefficient of such non-uniformly iced angle bars, or tower legs, one should divide the angle bar into smaller pieces for which ice thickness is assumed constant, and determine the drag coefficient as a function of position along the bar.

## **Acknowledgements**

This work was carried out within the framework of the NSERC/Hydro-Quebec/UQAC Industrial Chair on Atmospheric Icing of Power Network Equipment (CIGELE) and the Canada Research Chair on Engineering of Power Network Atmospheric Icing (INGIVRE) at Université du Québec à Chicoutimi. The authors would like to thank the CIGELE partners (Hydro-Québec, Hydro One, Réseau de Transport d'Électricité (RTE) and Électricité de France (EDF), Alcan Cable, K-Line Insulators, Tyco Electronics, Dual-ADE, and FUQAC) whose financial support made this research possible. The authors are grateful to Caroline Potvin for FT-IR analysis.

## References

- Air Force Geophysics Laboratory. 1985. Handbook of Geophysics and Space Environment. Ed. A. S. Jursa. United States Air Force
- Banitalebi Dehkordi, H., Farzaneh, M., Kollar, L.E., Van Dyke, P., 2011. Experimental Study of Spray Characteristics and its Uniformity under Different Icing Conditions, Proc. of 14th Int. Workshop on Atmospheric Icing of Structures, Chongqing, China, Paper P1\_32\_ID219.
- Bragg, M.B., 1988. Experimental aerodynamic characteristics of an NACA 0012 airfoil with simulated glaze ice, *J. Aircraft*, 25 (9), 849-854.
- Bragg, M.B., Loth, E., 2000. Effects of large droplet ice accretion on airfoil and wing aerodynamics and control, Technical report, U.S. Department of Transportation Federal Aviation Administration Final Report Office of Aviation Research, Washington DC, 20591.
- Cheng, K.Y., Wang, P.K. 2013. A numerical study of the flow fields around falling hails, *J. Atmospheric Research*, Volumes 132-133, 253-263.
- Cober, S. G., G. A. Isaac, and J. W. Strapp. 2001. Characterization of Aircraft Icing Environments That Include Supercooled Large Drops. *Journal of Applied Meteorol* 40: 1984–2002.
- Frisch, A. Shelby, Brooks E. Martner, Irina Djalalova, and Michael R. Poellot. 2000. Comparison of Radar/radiometer Retrievals of Stratus Cloud Liquid-water Content Profiles with in Situ Measurements by Aircraft. *Journal of Geophysical Research* 105 (D12) 15361.
- Hoerner, S.F., 1965. Practical information on aerodynamic drag and hydrodynamic resistance, Midland Park, N.J., 3<sup>rd</sup> ed.
- International Standards of Atmospheric Icing on Structures, ISO12494:2001(E).
- Jeck, R. K. 1996. Representative Values of Icing Related Variables Aloft in Freezing Rain and Freezing Drizzle, DOT/FAA/AR-TN95/119. Atlantic city.
- Jeck, R. K. 2002. Icing-Design Envelopes (14 CFR Parts 25 and 29, Appendix C) Converted to a Distance-Based Format, DOT/FAA/AR-00/30. Atlantic city.
- Kollar, L.E., Farzaneh, M., Karev, A.R., 2006. Modeling Droplet Size Distribution near a Nozzle Outlet in an Icing Wind Tunnel, *J. Atomization and Sprays*, 16 (6), 673-686.
- Kollar, L.E., Farzaneh, M., 2007. Modeling the evolution of droplet size distribution in two-phase flows, *International J. Multiphase Flow*, 33 (11), 1255-1270.
- Kollar, L.E., Farzaneh, M., 2009. Spray characteristics of artificial aerosol clouds in a low-speed icing wind tunnel, *J. Atomization and Sprays*, 19 (4), 387-405.
- Kollar, L.E., Farzaneh, M., 2010. Wind-tunnel investigation of icing of an inclined cylinder, *International J. Heat and Mass transfer*, 53 (5-6), 849-861.

- Kollar, L. E., Farzaneh, M., 2011. Modeling and Experimental Study of Variation of Droplet Cloud Characteristics in a Low-Speed Horizontal Icing Wind Tunnel, Chapter 3 in: *Wind Tunnels: Aerodynamics, Models and Experiments*, Nova Science Publishers, inc., Hauppauge, NY, pp. 93-127
- Lee, S., Bragg, M.B., 2003. Investigation of factors affecting iced-airfoil aerodynamics, *J. Aircraft*, 40 (3), 499-508.
- Lynch, F., Khodadoust, A., 2002. Effects of ice accretions on aircraft aerodynamics, *J. Aerospace Science*, 38 (3), 273-274.
- Politovich, M.K., 1989. Aircraft icing cause by large supercooled droplets, *J. Applied Meteorology*, 28, 856–868.
- Vargas, M., 2005. Current experimental basis for modeling ice accretions on swept wings, AIAA Paper 2005-5188.
- Vargas, M., Giriunas, J. A., Ratvasky, T. P., 2002. Ice accretion formations on a NACA 0012 swept wing tip in natural conditions, AIAA Paper 2002-0244.
- Yeo, D., Jones, N.P., 2011. Characterization of flow oblique to a circular cylinder with low aspect ratio using 3-D detached eddy simulation, *J. Wind Engineering and Industrial Aerodynamics*, 99 (11), 1117-1125.